

1 Experimental setup

Figure S1 provides a schematic for the setup and inter-connectivity of the electronics used to measure and control the single ^{31}P nuclear spin. The electronics reside at room-temperature, whilst the qubit device is mounted in a dilution refrigerator with electron temperature ~ 300 mK, and subject to static magnetic fields between 1.0 and 1.8 T. For our voltage pulses, we employed a compensation technique using a Tektronix AWG520, to ensure that the pulsing only shifted the donor electrochemical potentials but kept the SET island potential constant. The voltage V_p (see Fig. S1b) was applied directly to the top gate, while it was inverted and amplified by a factor K before reaching the plunger gate. The gain K was carefully tuned to ensure that the SET operating point moved along the top of the SET current peaks, as shown by the blue arrow in Fig. 1d of ref. 9. The SET current was measured by a Femto DLPCA-200 transimpedance amplifier at room temperature, followed by a voltage post-amplifier, a 6th order low-pass Bessel filter, and a fast digitizing oscilloscope.

The ESR excitations were produced by an Agilent E8257D microwave analog signal generator and the NMR excitations by an Agilent MXG N5182A RF vector signal generator. The two signals were combined at room-temperature with a power divider/combiner, before being guided to the sample by a semi-rigid coaxial cable (2.2 m in length with a loss of ~ 50 dB at 50 GHz). Gating of the ESR/NMR pulses was provided by the Tektronix AWG520, which was synchronized with the TG and PL pulses.

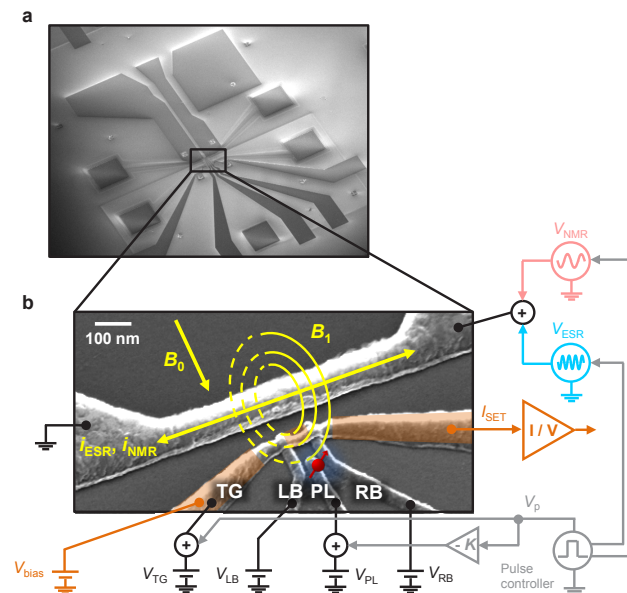


Figure 1: **Device structure and operation.** **a**, Scanning electron micrograph of the entire device. The on-chip broadband microwave transmission line is on the top-left side. **b**, Zoom of the active area, showing an implanted donor (donor as red arrow), the SET and the short-circuit termination of the microwave line.

2 Supplementary methods

Nuclear spin readout

We measure the nuclear spin state by toggling the microwave frequency ν_{ESR} between the two ESR resonances ν_{e1} and ν_{e2} , and attempting to adiabatically invert the electron spin from $|\downarrow\rangle$

to $|\uparrow\rangle$ 250 times at each frequency. The difference in the electron spin-up fraction $\Delta f_{\uparrow} = f_{\uparrow}(\nu_{e2}) - f_{\uparrow}(\nu_{e1})$ then reveals the nuclear spin state. The fast adiabatic passage is achieved by applying a frequency chirp centered about the ESR transition at a rate of 50 kHz and with a peak-to-peak deviation of 20 MHz.

SNR of nuclear spin readout experiment

The widths of the peaks in the nuclear spin readout histogram of Fig. 2d result from a combination of effects including: thermal broadening (caused by microwave induced heating), charge fluctuations (which alter the device biasing) and an imperfect adiabatic passage. These effects act to reduce the signal-to-noise ratio of the measurement and thus increase the readout error (Fig. 2e).

NMR experimental details

The NMR pulse protocol is very similar to that used in the nuclear spin readout measurement (Figs. 2a,b), with the primary difference being the inclusion of an 8 ms long RF excitation (see top inset of Fig. 3a). The nuclear resonance is detected by measuring the absolute difference in electron spin-up counts between the two ESR frequencies, $|\Delta f_{\uparrow}| = |f_{\uparrow}(\nu_{e2}) - f_{\uparrow}(\nu_{e1})|$, as a function of the NMR frequency ν_{NMR} . Off-resonance, we find the normal value $|\Delta f_{\uparrow}| \approx 0.4$, as observed in the nuclear spin readout experiment (Fig. 2b), because the nucleus retains its spin state for a very long time. Conversely, a resonant excitation quickly randomizes the nuclear spin state, causing $|\Delta f_{\uparrow}|$ to drop towards zero. ν_{n1} is found by applying an NMR burst before the ESR excitation (Fig. 3a), whereas for ν_{n2} we swap the order of ESR and NMR, to achieve a higher probability of having the electron spin $|\uparrow\rangle$. In order to observe the ν_{n0} resonance, we first ionize the donor before applying the RF pulse. The electron is then placed back onto the donor for the purpose of reading out the nuclear spin state.

Ramsey fringe and spin echo experiments

The Ramsey fringe pulse protocol begins with an initial $\pi/2$ pulse to put the nuclear spin in an equal superposition of $|\uparrow\rangle$ and $|\downarrow\rangle$, or equivalently, in the XY-plane on the Bloch sphere. We let it evolve for a time τ before executing another $\pi/2$ pulse and performing a measurement on the nuclear spin (see Fig. 4b for a Bloch sphere state evolution). We repeat the sequence 200 times and then step τ , with the acquisition of each τ occurring over ~ 3 minutes. The spin is intentionally detuned from resonance so that during the period of free evolution, a phase is accumulated between the states $|\uparrow\rangle$ and $|\downarrow\rangle$. Consequently, interference fringes/oscillations are observed in the recovered nuclear spin flip probability as a function of τ (Fig. 4c).

The spin echo is a simple extension of the Ramsey fringe sequence, where we perform a π rotation in the middle of the free evolution period of Fig. 4a. This modified sequence (Fig. 4d) is also known as a Hahn echo (refer to Fig. 4e for a Bloch sphere representation).

Optimizing the nuclear spin readout time

The nuclear spin readout fidelity depends on the measurement time T_{meas} , which is given by the number of single-shot electron spin readout events acquired per measurement. The larger the number of electron spin single-shots taken, the lower the SNR-limited readout error will be. However, a trade-off exists in that the longer measurement duration results in a greater chance of a nuclear spin quantum jump occurring during readout. In Figs. 2a,b, 250 shots resulted in a 260 ms measurement duration and a SNR-limited readout error of 2×10^{-7} (as

extracted from Fig. 2e). By decreasing the number of shots to 100, we were able to perform the measurement in less than half of the time ($T_{\text{meas}} = 104$ ms) with an increased, but still relatively low SNR-limited error of 2×10^{-5} . We find that 100 shots provides a near optimal tradeoff between nuclear spin quantum jump occurrence and the SNR-limited readout error.

3 Calculation of the electron g-factor

As shown in ref. 23, we can write the energies for the states $|\uparrow\uparrow\rangle$, $|\uparrow\downarrow\rangle$, $|\downarrow\downarrow\rangle$ and $|\downarrow\uparrow\rangle$ as:

$$\begin{aligned} |\downarrow\uparrow\rangle : E_{\downarrow\uparrow} &= \frac{-\sqrt{(\gamma_+ B_0)^2 + A^2} - A/2}{2} \\ |\downarrow\downarrow\rangle : E_{\downarrow\downarrow} &= \frac{-\gamma_- B_0 + A/2}{2} \\ |\uparrow\downarrow\rangle : E_{\uparrow\downarrow} &= \frac{\sqrt{(\gamma_+ B_0)^2 + A^2} - A/2}{2} \\ |\uparrow\uparrow\rangle : E_{\uparrow\uparrow} &= \frac{\gamma_- B_0 + A/2}{2} \end{aligned}$$

where $\gamma_{\pm} = \gamma_e \pm \gamma_n$, $\gamma_{e(n)}$ is the gyromagnetic ratio for the electron (nucleus) as defined in the main text, B_0 is the external magnetic field and A is the hyperfine constant. The states $|\uparrow\downarrow\rangle$ and $|\downarrow\uparrow\rangle$ are good approximations to the actual eigenstates and become exact in the limit $\gamma_e B_0 \gg A$. We can express the nuclear spin resonance frequencies of Fig. 1b as:

$$\begin{aligned} \nu_{n1} = E_{\downarrow\downarrow} - E_{\downarrow\uparrow} &= \frac{A + \sqrt{(\gamma_+ B_0)^2 + A^2} - \gamma_- B_0}{2} \\ \nu_{n2} = E_{\uparrow\uparrow} - E_{\uparrow\downarrow} &= \frac{A - \sqrt{(\gamma_+ B_0)^2 + A^2} + \gamma_- B_0}{2} \end{aligned}$$

Using measured values of the NMR frequencies (ν_{n1} and ν_{n2}), along with the known values of the ^{31}P electron and nuclear gyromagnetic ratios [23], an accurate calibration of the external field B_0 can be made,

$$B_0 = \frac{\Delta\nu_n \gamma_- + \sqrt{\Delta\nu_n^2 \gamma_+^2 - 4\gamma_e \gamma_n A^2}}{4\gamma_e \gamma_n}$$

where $\Delta\nu_n = \nu_{n1} - \nu_{n2}$ and $A = \nu_{n1} + \nu_{n2}$. With the experimentally determined ESR transition frequencies (ν_{e1} and ν_{e2}), we can then calculate the electron g-factor,

$$g = \frac{h\bar{\nu}_e}{\mu_B B_0}$$

where $\bar{\nu}_e = (\nu_{e1} + \nu_{e2})/2$, h is Planck's constant and μ_B is the Bohr magneton. Of course, the electron gyromagnetic ratio $\gamma_e = g\mu_B/h$, which is used in the calculation of B_0 , itself depends on the electron g-factor. We must therefore calculate B_0 and g recursively. After extracting the g-factor from each data point in Fig. 3b using the measured values of ν_{n1} , ν_{n2} , ν_{e1} and ν_{e2} , we find an average value of $g = 1.9987(6)$, within $\sim 0.01\%$ of the bulk value of 1.9985 [24].

4 Nuclear spin lifetime measurements

We probe the nuclear spin flip rates as well as establish the cause of the $|\uparrow\rangle \rightarrow |\downarrow\rangle$ transition by modifying the readout pulse protocol to include a resonant tunneling phase, during which random tunneling of $|\downarrow\rangle$ electrons back and forth between the ^{31}P donor and the SET island can occur (see Section 5). This process is observed to decrease the $|\uparrow\rangle$ state lifetime (Fig. 2c) relative to that found for the nuclear spin readout experiment of Fig. 2b. In Fig. 2f we plot the lifetime of the nuclear $|\downarrow\rangle$ and $|\uparrow\rangle$ states as a function of the rate of donor ionization/neutralization $\Gamma_{\text{ion/neut}}$. We find that the lifetime of the nuclear $|\downarrow\rangle$ is approximately independent of $\Gamma_{\text{ion/neut}}$, as expected if the process is dominated by electron-nuclear spin flip-flops with phonon emission [26]. Conversely, the lifetime of the nuclear $|\uparrow\rangle$ is longer and inversely proportional to $\Gamma_{\text{ion/neut}}$.

The physical mechanism of the $|\uparrow\rangle \rightarrow |\downarrow\rangle$ flips can be traced back to the form of the hyperfine coupling between the electron (S) and nuclear (I) spins. The Hamiltonian of the donor system is given by:

$$\mathcal{H}(t) = \gamma_e B_0 S_z - \gamma_n B_0 I_z + A(t) \left[S_z I_z + \frac{1}{2}(S_+ I_- + S_- I_+) \right] \quad (1)$$

where S_{\pm} (I_{\pm}) represents the electron (nuclear) raising/lowering operator and the other parameters here have already been described in the main text. $A(t)$ toggles between 0 and 114.3 MHz depending whether the donor is ionized or neutral, respectively. It is clear from equation (1) that when $A = 0$ (ionized donor) both S_z and I_z are constants of motion, and the exact eigenstates are the tensor products of the up/down electron-nuclear states. Conversely, for $A \neq 0$ (neutral donor) the exact eigenstates become:

$$\begin{aligned} |\varphi_1\rangle &= \cos(\eta/2) |\downarrow\uparrow\rangle - \sin(\eta/2) |\uparrow\downarrow\rangle \\ |\varphi_2\rangle &= |\downarrow\downarrow\rangle \\ |\varphi_3\rangle &= \cos(\eta/2) |\uparrow\downarrow\rangle + \sin(\eta/2) |\downarrow\uparrow\rangle \\ |\varphi_4\rangle &= |\uparrow\uparrow\rangle \end{aligned}$$

where $\tan(\eta) = A/(\gamma_+ B_0)$. The non-secular terms in the expanded hyperfine coupling, $S_+ I_- + S_- I_+$, create a slight mixing of the states $|\downarrow\uparrow\rangle$ and $|\uparrow\downarrow\rangle$ of the uncoupled or ionized system. If we start in an eigenstate of the coupled system $|\varphi_1\rangle$, then each ionization/neutralization event accumulates a small probability of flipping from $|\uparrow\rangle \rightarrow |\downarrow\rangle$ given by $\sin(\eta/2)^2 \approx 1.3 \times 10^{-6}$ for $B_0 \approx 1.8$ T. This is in excellent agreement with the value of p as extracted from the data in Fig. 2f. We note that the reverse process $|\downarrow\rangle \rightarrow |\uparrow\rangle$ is equally possible, but it is not directly observable in our experiments due to the predominance of the flipping mechanism originating from the phonon modulation of the hyperfine coupling, which does not depend on the ionization/neutralization rate.

5 Pulse protocol to include a resonant tunneling phase

We controlled the electron ionization/neutralization rate $\Gamma_{\text{ion/neut}}$ by modifying the nuclear spin readout protocol. Here we add to the measurement an additional phase, where we align the donor electron spin-down electrochemical potential μ_{\downarrow} with that of the electrons in the SET island μ_{SET} . During this phase (where $\mu_{\downarrow} \approx \mu_{\text{SET}}$) spin-down electrons tunnel back and forth between the donor and the SET island (see Figs. S2a-b). The corresponding pattern of I_{SET} (Fig. S2c) resembles a random telegraph signal (RTS). Varying the duration of the resonant tunneling phase τ_{res} provides control of the donor ionization/neutralization rate $\Gamma_{\text{ion/neut}}$, which allows us to gain insight to the nuclear spin-up flip process.

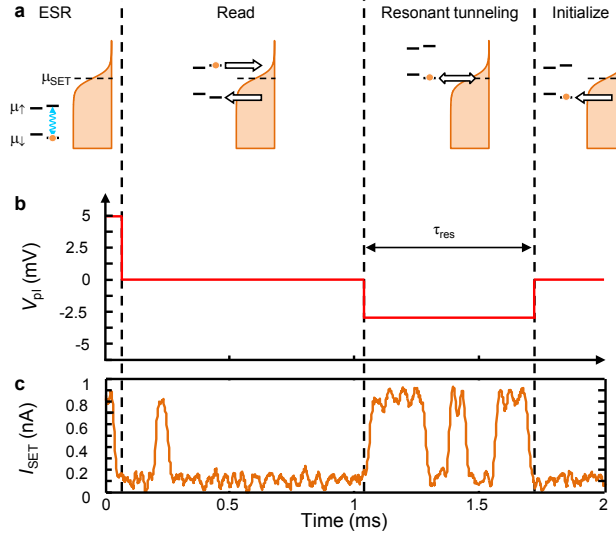


Figure 2: **Pulse protocol for the modified quantum jumps measurement.** **a**, Sketch of the (spin-dependent) electrochemical potentials of the donor electron $\mu_{\downarrow/\uparrow}$ and SET μ_{SET} during the measurement process. The pulse levels are chosen such that: $\mu_{\downarrow,\uparrow} \ll \mu_{\text{SET}}$ for the ESR phase, $\mu_{\downarrow} < \mu_{\text{SET}} < \mu_{\uparrow}$ for the read and initialize phases, and $\mu_{\downarrow} \approx \mu_{\text{SET}}$ for the resonant tunneling phase. **b**, Plunger voltage pulse level and timing scheme. **c**, Sample response of the current through the SET I_{SET} to the above pulse protocol. The current peaks during the resonant tunneling phase *do not* correspond to readout of $|\uparrow\rangle$ electrons, but arise because of the allowed tunneling of $|\downarrow\rangle$ electrons to and from the SET island.

6 Nuclear spin flip rate error calculations

Here we describe the estimation of errors for the nuclear spin flip rate measurements of Fig. 2f. Each point in Fig. 2f represents the inverse decay time (the rate, $\Gamma_{\uparrow/\downarrow}$) of a histogram of flip times (t_{flip}) extracted from data similar to that in Figs. 2b,c (see Fig. S3).

The uncertainty in the flip rate comes from having a finite sample size of flip times. With a small sample size, the choice of histogram bin size can affect the apparent $\Gamma_{\uparrow/\downarrow}$. We first calculate an optimum bin width $W = 2(IQR)L^{-\frac{1}{3}}$, where IQR is the interquartile range and L is the sample size. We then extract $\Gamma_{\uparrow/\downarrow}$ from a number of histograms using a range of bin sizes centered around the optimum. For each we also find the 95% confidence interval ε_{fit} of the fitting parameter $\Gamma_{\uparrow/\downarrow}$. The total error (vertical bar) is then given by equation (2), which is the geometric sum of: (i) the 95% confidence interval ε_{bin} of the fluctuations in $\Gamma_{\uparrow/\downarrow}$ resulting from different histogram bin sizes; and (ii) the average ε_{fit} from all histograms. We neglect experimental error due to the sampling resolution of the quantum jumps measurements, since the minimum nuclear flip time (~ 1 minute) is much greater than the maximum sample time (~ 1.5 seconds for the longest resonant tunneling measurement).

The error in $\Gamma_{\text{ion/neut}}$ (horizontal bar) results from small fluctuations in the sample biasing over the duration of each measurement. For each $\Gamma_{\uparrow/\downarrow}$ data point, we count the total number of ionization/neutralization events per single-shot and calculate the standard deviation over all shots $\sigma_{\text{ion/neut}}$. We then convert $\sigma_{\text{ion/neut}}$ into a rate by dividing by the length of each single-shot.

$$\varepsilon = \sqrt{\varepsilon_{\text{bin}}^2 + \bar{\varepsilon}_{\text{fit}}^2} \quad (2)$$

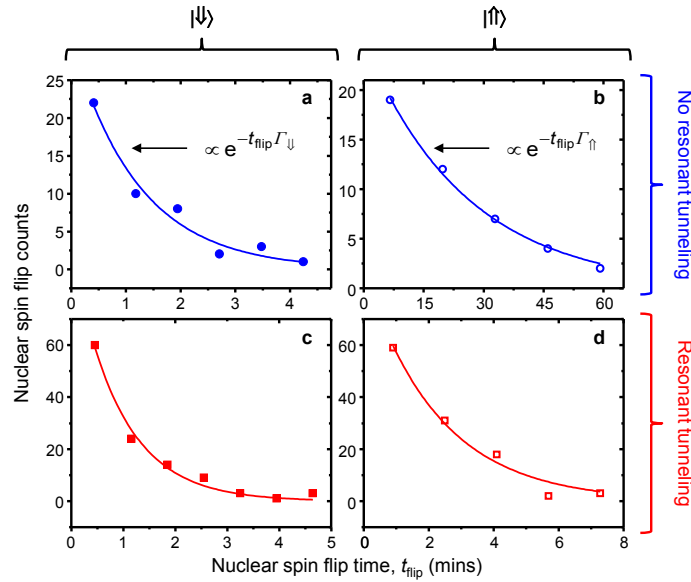


Figure 3: **Nuclear spin-up and spin-down flip time histograms.** **a-b**, Nuclear spin-down (**a**) and spin-up (**b**) flip time histograms, extracted from the data of Fig. 2b in the main text. Exponential fits are used to determine the nuclear spin flip rates $\Gamma_{\uparrow/\downarrow}$. **c-d**, Nuclear spin-down (**c**) and spin-up (**d**) flip time histograms, extracted from the data of the resonant tunneling experiment of Fig. 2c. It is evident from the histograms that the addition of the resonant tunneling phase drastically increases Γ_{\uparrow} , but has little effect on Γ_{\downarrow} .

7 Quantum non-demolition readout

In general, a QND measurement is obtained if the Hamiltonian \mathcal{H}_{int} , describing the interaction between observable and measurement apparatus, commutes with the observable [11]. In our case, the observable is the z projection of the nuclear spin state I_z , while the measurement apparatus is the electron spin. The QND condition, $[I_z, \mathcal{H}_{\text{int}}] = 0$, would require a hyperfine coupling of the form $AS_z I_z$. The physical phenomena responsible for the observed nuclear spin quantum jumps originate from the measurement through the electron spin (see Section 4), and can be viewed as a deviation from QND ideality. The isotropic hyperfine coupling contains the terms $A_{\parallel}/2(S_+ I_- + S_- I_+)$, which do not commute with I_z . In addition any anisotropic part of the hyperfine tensor \underline{A} (e.g., $A_{\perp} S_z I_x$) also does not commute with I_z . Here, A_{\parallel} (A_{\perp}) represents the diagonal (off-diagonal) components of the hyperfine tensor \underline{A} . For the nuclear $|\uparrow\rangle$ state, this results in a lifetime $T_{\uparrow} = 1500(360)$ s. For the nuclear $|\downarrow\rangle$ state, the cross-relaxation process - caused by phonons modulating the hyperfine coupling - also introduces a term that does not commute with I_z , yielding a lifetime $T_{\downarrow} = 65(15)$ s.

8 Rotation angle error

Here we determine the rotation angle error and control fidelity for the ionized nuclear spin, using the method outlined in ref. 31. We employ two different dynamical decoupling sequences to measure the coherence time T_2 ; the Carr Purcell (CP) sequence and the Carr Purcell Meiboom Gill (CPMG) sequence. The CP protocol is a simple modification on the Hahn echo (Fig. 4d), where the single refocusing π pulse is replaced with a series of π rotations separated from one another by a delay 2τ (see inset of Fig. S4b). In the CP sequence, all pulses (including the initial and final $\pi/2$ rotations) are about the same axis on the Bloch sphere, and their associated

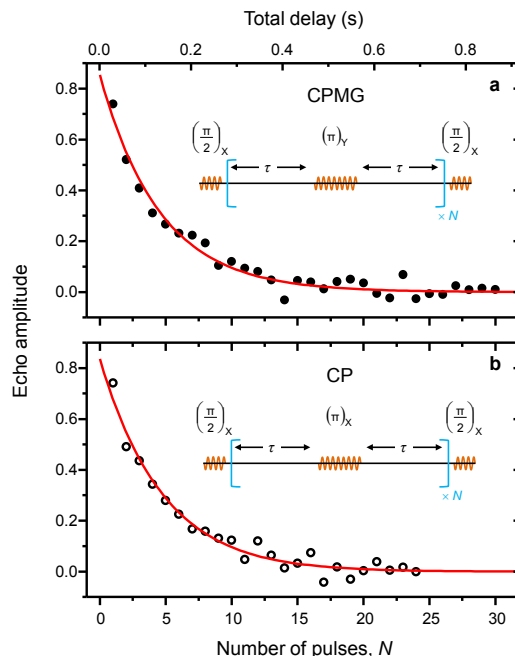


Figure 4: **Coherence measurements for extracting the rotation angle error.** **a**, A Carr Purcell Meiboom Gill (CPMG) experiment where we plot the echo amplitude as a function of the number of π pulses applied N , with a fixed delay τ . We calculate the signal amplitude using simulated quadrature detection [10]. The CPMG sequence is shown as an inset. The fit to the data is a simple exponential decay of the form $y = \exp(-2N\tau/T_{2,\text{CPMG}})$ **b**, Echo decay from a Carr Purcell (CP) sequence (see inset), which differs from the CPMG sequence in the axis about which the π rotations are performed. The fit through the data is discussed in the text. Both the CPMG and CP measurements were obtained over 36 sweeps of N , where in a single sweep we perform 40 repetitions of the pulse sequence for each N . The echo decay amplitudes were ~ 0.85 for both the CPMG and CP experiments, we attribute this reduction to a miscalibration of the $\pi/2$ pulses (which were simply assumed to be half the duration of a π rotation), systematic phase errors producing rotations that were not completely orthogonal and the occurrence of nuclear spin quantum jumps during the measurements.

errors are additive. The CPMG sequence remedies the problem of pulse error accumulation by performing the π rotations about an orthogonal axis (inset of Fig. S4a), in our case the Y axis.

In order to find the error involved in a single π pulse, we monitor the decay of the CPMG echo signal (Fig. S4a) as we increase N , the number of π pulses in the sequence. Here τ is fixed at 14.4 ms, and an exponential fit to the data provides a coherence time of $T_{2,\text{CPMG}} = 131 \pm 7$ ms. We repeat the measurement with the CP sequence and observe the decay of Fig. S4b. Because the CP sequence accumulates pulse errors, the decay should be attenuated by an additional factor given by $\exp(-\sigma^2 N^2/4)$ [31], where σ is the standard deviation of the error (in radians) for a single π rotation. Here it is assumed that the mean flip angle error is negligible, and we have gone to great lengths to ensure that rotation errors due to systematic off-resonance or pulse timing effects were kept to a minimum. We periodically performed Ramsey fringe measurements to ensure that we were tuned within 100 Hz of the resonance frequency, and Rabi oscillations were regularly taken to calibrate the π pulse duration.

For measurements on bulk-doped samples, σ originates from the inhomogeneity of the RF or microwave field over the sample volume. Because we measure only a single donor, σ here would more likely result from slow power fluctuations of the RF source. Fitting the CP data with a function of the form $y = \exp(-2N\tau/T_{2,\text{CPMG}}) \exp(-\sigma^2 N^2/4)$, where $T_{2,\text{CPMG}}$ is the

coherence time as extracted from the CPMG measurement, we find by considering the best-case $T_{2,\text{CPMG}}$ of 138 ms a σ of 0.05 radians ($\sim 3^\circ$). Note that by using the standard error in the fitting parameter $T_{2,\text{CPMG}}$ to extract σ , we obtain an uncertainty and can only conclude that the control fidelity $F_C = 1 - \sigma/180^\circ$ is greater than 98%. A more accurate specification of F_C would require the acquisition of many more data sets, which was impractical considering the timescale over which the measurements of Fig. S4 were obtained (~ 70 hours).

Supplementary references

31. Morton, J. J. L. *et al.* Measuring errors in single-qubit rotations by pulsed electron paramagnetic resonance. *Phys. Rev. A* **71**, 012332 (2005).